Direct Observation of Nanoscale Size Effects in Ge Semiconductor Nanowire Growth

Shadi A. Dayeh* and S. T. Picraux*

Center for Integrated Nanotechnologies (CINT), Los Alamos National Laboratory, Los Alamos, New Mexico 87545

ABSTRACT Progress in the synthesis of semiconductor nanowires (NWs) has prompted intensive inquiry into understanding the science of their growth mechanisms and ultimately the technological applications they promise. We present new results for the size-dependent growth kinetics of Ge NWs and correlate the results with a direct experimental measurement of the Gibbs−Thomson effect, a measured increase in the Ge solute concentration in liquid Au−Ge droplets with decreasing diameter. This nanoscale-dependent effect emerges in vapor−liquid−solid Ge NW growth and leads to a decrease in the NW growth rate for smaller diameter NWs under a wide range of growth conditions with a cutoff in growth at sufficiently small sizes. These effects are described quantitatively by an analytical model based on the Gibbs−Thomson effect. A comprehensive treatment is provided and shown to be consistent with experiment for the effect of NW growth time, temperature, pressure, and doping on the supersaturation of Ge in Au, which determines the growth rate and critical cutoff diameter for NW growth. These results support the universal applicability of the Gibbs−Thomson effect to sub-100 nm diameter semiconductor NW growth.

KEYWORDS Nanowire, silicon, germanium, size-dependent growth, vapor-liquid-solid growth, Gibbs-Thomson

Semiconductor nanowires (NWs) allow the realization of one-dimensional (1D) structures that exhibit unusual electronic and optical properties, as well as unique device architectures. Metal-catalyzed growth of NWs with high aspect ratio between their lengths and diameters and superb control over their morphology are typically grown by the vapor−liquid−solid (VLS) mechanism.[1−4] In the VLS growth process, gas precursors containing reactant material catalytically decompose and incorporate at a metal nanoparticle surface forming a liquid droplet. This liquid droplet continues to adsorb decomposing solute atoms from the vapor, leading to a supersaturated state at which time crystallization of the semiconductor occurs at the liquid−solid interface resulting in 1D NW growth. Since the diameter, and consequently the electronic and optical properties of NWs, are dependent on the size of the metal nanoparticle, understanding and controlling the diameter-dependent growth behavior in semiconductor NWs is important. In some material systems, such as compound semiconductors where two different precursors are used, heterogeneous precursor/substrate and precursor/NW-sidewall reactions as well as gas phase precursor reactions can limit mass transport (typically of group III adatoms) to the liquid particle, thereby introducing additional factors in controlling the NW growth rate and morphology.[5,6] These additional factors complicate the isolation of size dependent effects, such as the Gibbs−Thomson effect, at small diameters in compound semiconductor systems.

Elemental semiconductors on the other hand typically utilize a single precursor such as SiH_4 for Si NWs[7] and GeH_4 for Ge NWs.[8] In addition, their growth is carried out at low temperatures and pressures such that the precursors are not usually subject to complex mixed reactions such as in III−V NWs prior to arriving to the liquid droplet. This makes Si and Ge NWs well suited for studying the kinetics of the VLS mechanism and the applicability of the Gibbs−Thomson effect, a reduction of supersaturation for smaller diameter liquid growth seeds due to an increase in the solid NW chemical potential, to diameter-dependent growth behavior. Previously NW growth studies of the diameter-dependent growth rate have primarily focused on Si NWs.[9−16] In some cases, inconsistencies in size-dependences have been observed when the growth was performed under low SiH_4 or Si_2H_6 partial pressures due to Au loss by diffusion from the Au seed at the NW tips, or due to the presence of oxide masks and contaminants on the growth substrate surface.[15,16] We observe that it is easier to grow epitaxially vertical Ge NWs on Ge (111) surfaces, in contrast to the typically mixed vertical and inclined NW orientations for Si NW growth on Si (111) using SiH_4 or Si_2H_6,[16] leading to mostly ⟨111⟩-oriented vertical wires for all Ge NW diameters down to sub-10 nm diameters,[17] thereby excluding growth direction or other orientation effects on NW growth rates. Currently, no diameter-dependent studies have been reported for Ge NWs, the increasingly important electronic counterpart of Si with higher electron and hole mobilities[18] and the focus of this study.

In this article, we present a detailed study of the diameter dependent growth rate of Ge NWs and also present the first direct evidence of the Gibbs−Thomson effect by correlating observed diameter-dependent growth rates with *in situ*
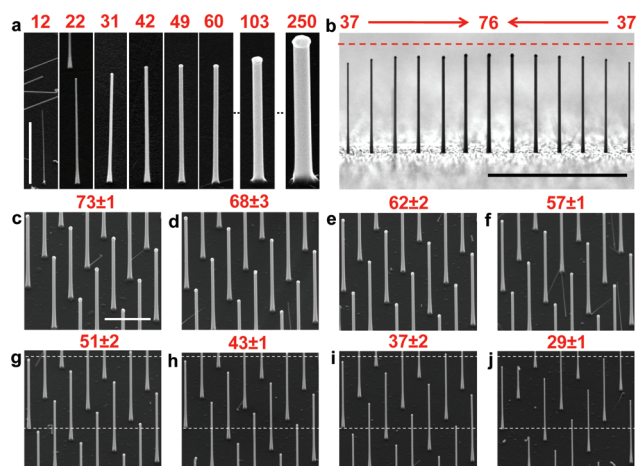
FIGURE 1. Ge nanowires with controllable diameter. (a) FE-SEM images of vertical NWs grown for 15 min at 276 °C from randomly dispersed Au colloids of nominal diameter 10, 20, 30, 40, 50, 60, 100, and 250 nm. The resultant measured average NW diameter (nm) is indicated at the top of each SEM image. The images were taken at the same magnification and the angle-corrected scale bar (far left side, vertical bar) is 1.41 μm. (b) Linear array of Ge NWs grown from lithographically patterned Au dots. The dashed red line highlights the systematic changes in NW length at different diameters. Scale bar is 3 μm. (c−j) Arrays of uniformly sized Ge NWs grown from Au dots with 100, 90, 80, 70, 60, 50, 40, and 30 nm diameter, 20 nm thickness, and 1 μm spacing, grown for 10 min at 276 °C. The resulting average NW diameters and statistical standard deviations are indicated at the top of each SEM image. Scale bar is 1 μm. The dashed white lines in (e−h) serve as a guide-to-the-eye for comparing the left-most NW lengths.

measurements of the Ge atomic fraction in different diameter liquid Au nanoparticles atop the same set of NWs. Previously, observations of reduced growth rates for Si NWs at small diameters have been used to infer the Gibbs−Thomson effect, but size-dependent changes in the solute fraction in different diameter Au growth seeds have not been systematically measured. We combine model and experiment based on these results to show excellent agreement of the diameter-dependent growth kinetics at small diameters with that predicted from the Gibbs−Thomson effect under all growth conditions, including the presence and absence of doping precursors (PH_3 and B_2H_6), different growth temperatures, and different GeH_4 precursor partial pressures. We also examine the consequences of this model for the minimum diameter NWs predicted to grow - the cutoff diameter for NW growth - as a function of growth temperature, pressure, and surface energies, and find good agreement with experiment.

In our growth studies for Ge NWs at the lowest temperature, we use a two-step process[19] where an ∼1.5 min NW nucleation step was performed at ∼366 °C and the temperature was ramped down in 3 min to ∼276 °C where NW elongation took place.[20] Figure 1 shows field-emission scanning electron microscope (FE-SEM) images of undoped Ge NWs grown on Ge(111) surfaces. The Ge NW length decreases with decreasing diameter for a given growth time as shown in Figure 1a for NWs grown from solution-

deposited Au nanoparticles. Similarly, for Ge NWs grown from lithographically patterned Au dots, smaller diameter Au dots lead to shorter NWs as demonstrated in Figure 1b. The same diameter dependent growth rate is observed for NWs grown in arrays with similar dot diameters and variable interwire spacing (Supporting Information Figure S1). For NW arrays with constant 1 μm interwire spacing, 100 μm spacing between arrays, and constant dot sizes, those NWs from arrays of smaller Au dot diameters resulted in shorter NWs than those of larger Au dot diameters as shown in Figure 1c−j. Variation in only the interwire spacing (0.5−4 μm, see Supporting Information Figure S2) for a constant Au dot size had negligible effect on the growth rate, thus excluding the possibility of synergetic spacing effects here on the growth rate as was observed for GaP NWs where the molar group-V/group-III ratio modifies the Ga diffusion length and therefore the growth rate.[5] These diameter-dependent growth rate results for Ge are in qualitative agreement with those for Si and SiGe alloys in refs 9−13 and with those of ref 14 if only small diameter NWs are considered. Previous studies of Si NW growth have shown that large diameter NWs (exceeding 100 nm) can display increased incubation time effects and thus lead to reduced lengths with increasing diameter.[21] Our systematic studies discussed here focus on sub-100 nm diameter Ge NWs and no incubation time effects are observed over the time scale and growth conditions used in our experiments (see Supporting Information Figure S5). Our higher nucleation temperature used in these studies ensures rapid and highly efficient nucleation that avoids incubation time effects and leads to optimal control over the Ge NW morphology and epitaxy as demonstrated in Figure 1 (also Supporting Information Figures S1−S4).

Figure 2a shows the average NW length, L, as a function of diameter, d, for nominally undoped Ge NWs grown from Au seeds at 276 °C for different elongation times in steps of 5 min. The NW lengths show a persistent decrease in the NW length with diameter and their elongation was linear with time for a given diameter (see also Supporting Information Figure S6). For diameters less than 20 nm, measurements were taken from epitaxial (111) oriented NWs grown from e-beam patterned Au film regions on the Ge(111) surface just outside the patterned Au dot arrays and grown simultaneously with the arrays (see Supporting Information Figure S7). The growth rates measured for the vertical (111)-oriented Ge NWs gave consistent results whether from lithographically patterned Au dots or films and the use of patterned Au films allowed the NW growth rate data to be extended to smaller diameters than could be achieved by the Au dots alone. All the growth rate data shown are for lithographically defined Au dots and films. The Au colloids (Figure 1a) gave similar rates but were only carried out in one run to demonstrate that this size dependent effect is independent of the method used to form the Au growth seeds. In what follows, we first analyze the growth behavior for typical low-temperature growth conditions for undoped
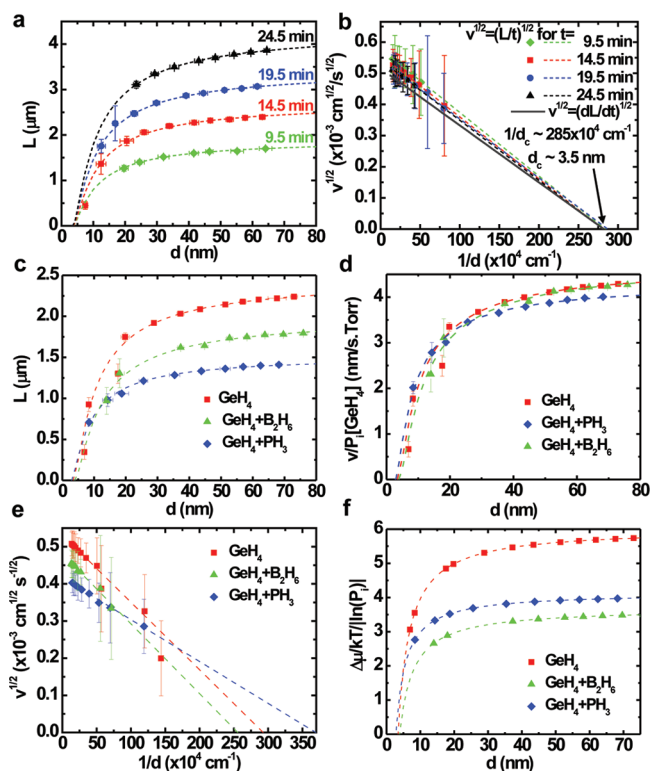
FIGURE 2. Plots of Ge NW growth rate with and without doping illustrating applicability of the Gibbs−Thomson effect on their growth. (a) Plot of the NW length as function of diameter with a $P[GeH_4] = 0.6$ Torr for different growth times at the low temperature step ($t(276\ °C) = 5, 10, 15$, and 20 min) resulting in a linear increase of NW length with time for all diameters (also see Supporting Information Figure S6). (b) Plot of the square root of the growth velocity for the data shown in (a) calculated using $v = L/t$ and using $v = dL/dt$ showing convergence of all data to the same cutoff diameter of ~3.55 nm. (c) Plot of the NW length as function of diameter with a $P[GeH_4] = 0.6$ Torr (red squares) with $P[GeH_4] = 0.4$ Torr and $P[PH_3] = 65.3\ \mu$Torr (blue diamonds), and $P[GeH_4] = 0.48$ Torr and $P[B_2H_6] = 39\ \mu$Torr (green triangles).[34] The dashed lines in all plots are calculated growth rates according to eq 3. (d) Plot of the growth rate normalized by the GeH_4 partial pressure showing a reduction in the growth rate when PH_3 is present during growth. (e) Plot of the square root of the growth rate as a function of inverse diameter illustrating good agreement of Ge NW growth with the Gibbs−Thomson effect under different growth conditions. (f) Plot of the supersaturation in the seed particle as a function of particle diameter according to eq 1 for our doped and undoped Ge NWs. Since $P[GeH_4]$ varied for doped and undoped growth experiments and because $\Delta\mu \propto \ln(P_i)$ (see Supporting Information eq S1), plots of the supersaturation in (f) are normalized by $\ln(P_i)$.

Ge NWs and then discuss the modifications to this behavior with the addition of dopants and with changes in growth pressure and temperature. The Gibbs−Thomson effect provides a general relationship between the curvature of small droplets, such as the liquid alloy growth seeds employed for VLS NW growth, and their vapor pressure and chemical potential. This finite-size effect has important implications for nanoscale systems. For example, it causes a strong depression of the freezing point of liquids dispersed within porous materials,[22] and it governs Ostwald ripening,[23] the growth of large particles at the expense of smaller ones in polydispersed ensembles.

Due to the Gibbs−Thomson effect, the supersaturation $\Delta\mu$, which is the difference in the chemical potential of Ge atoms in the vapor and solid phases, that is, the driving force for Ge NW growth, becomes diameter dependent according to[24]

$$\Delta\mu = \Delta\mu_0 - \frac{4\Omega\alpha_{vs}}{d} \tag{1}$$

where $\Delta\mu_0$ denotes the supersaturation in the planar limit (i.e., $d \rightarrow \infty$), Ω is the atomic volume of the growth species, d is the diameter of the NW below the liquid droplet, and α_{vs} is the average surface energy density of the NW surface facets. According to eq 1, a decrease in diameter leads to a progressive reduction in supersaturation and ultimately $\Delta\mu = 0$, that is, the complete suppression of growth, at a cutoff diameter

$$d_c = 4\Omega\alpha_{vs}/\Delta\mu_0 \tag{2}$$

While Givargizov and Chernov have empirically found a quadratic power dependence of growth rate on supersaturation,[25] more detailed analytical studies have recently debated this finding with both linear and quadratic dependencies suggested.[26−32] Through detailed modeling that took into account the Gibbs−Thomson effect and nucleation-mediated growth, Dubrovskii and Sibirev found that the quadratic dependence of growth rate on supersaturation is valid when adatom surface diffusion on the NW surface is negligible,[26] a situation that applies here for Ge NW growth. In addition, a square dependence of the growth rate on supersaturation is further supported from our pressure dependent growth studies as discussed later in this paper. Therefore, we take the NW growth velocity, $v = dL/dt$, to depend quadratically on the supersaturation[26] in the present case, $v = b(\Delta\mu/kT)^2$, where b is a kinetic coefficient of crystallization, k is Boltzmann's constant, and T is the temperature. Thus, eq 1 can be rearranged as[25]

$$\sqrt{v} = \sqrt{b}\frac{\Delta\mu_0}{kT} - \sqrt{b}\frac{4\Omega\alpha_{vs}}{kT}\frac{1}{d} \tag{3}$$

By fitting eq 3 to our experimental data (Figure 2b), we can determine values for $\Delta\mu_0$, b, and the cutoff diameter, d_c, below which NW growth ceases.[33] Here, both assignments of the growth velocity as $v = dL/dt$ or $v = L/t$ (total NW length divided by the total growth time) resulted in a similar cutoff diameter $d_c \sim 3.5$ nm for all growth times used in Figure 2a. Namely, we obtain $d_c = 3.5, 3.55, 3.48$, and 3.55 nm for 9.5, 14.5, 19.5, and 24.5 min growth times (using $v = L/t$) and a $d_c = 3.54$ nm using ($v = dL/dt$). This

TABLE 1. Calculated Critical Diameters, Pressure-Normalized Supersaturation Values, and Kinetic Coefficients Based on Measured Results for Ge NWs Grown with and without Dopants at 276 °C Using Equations 2 and 3

	d_c (nm) $\pm$ 0.4	$\Delta\mu_0$ (meV) $\pm$ 17	$\Delta\mu_0/kT/\ln(|P_i|) \pm 0.7$	$b^{1/2}\alpha_{vs}$ (10^{-8}J/cm$^{3/2}$/s$^{1/2}$) $\pm$ 0.7
GeH$_4$	3.4	145	6.0	1.5
GeH$_4$ + B$_2$H$_6$	3.9	127	4.1	1.6
GeH$_4$ + PH$_3$	2.8	177	3.7	0.98

strong agreement in cutoff diameter extraction justifies the use of $v = L/t$ in subsequent parts of this paper.

It is of particular interest to identify mechanisms that lower the cutoff diameter, that is, could be employed to achieve ultrathin NWs expected to show pronounced quantization effects due to carrier confinement. Equation 2 suggests that an increase in the bulk supersaturation, $\Delta\mu_0$, or a lowering of the surface tension, α_{vs}, of the NW facets could have this effect. While it is difficult to vary $\Delta\mu_0$ independently in chemical vapor deposition without compromising the NW nucleation and morphology[35] (Supporting Information Figure S8), we have explored this possibility of changing α_{vs} by adding small amounts of dopant precursors (PH$_3$ and B$_2$H$_6$) to the GeH$_4$ gas during NW growth (Figure 2c). To our knowledge an influence of dopant precursors on the Gibbs-Thomson effect has not previously been reported. When normalized to the GeH$_4$ partial pressure (Figure 2d), corresponding to the flux of GeH$_4$ to the Au droplet surface, the normalized growth rate, $v/P_i = L/tP_i$, is slightly lowered in the presence of B$_2$H$_6$ at small diameters (leading to slightly larger d_c, Table 1) and a new interesting behavior in the diameter-dependent growth rates is observed with the addition of PH$_3$. With PH$_3$, v/P_i is lower than that of undoped NWs for $d \geq 20$ nm (progressively changing from a ~1% reduction at $d = 20$ nm to ~6.5% at $d = 80$ nm), while higher normalized growth rates are obtained for $d < 20$ nm (again changing from a ~2% increase at $d = 15$ nm to ~22% at $d = 7.5$ nm). Since the normalized supersaturation to partial pressure $\Delta\mu_0/kT/|\ln(P_i)|$ ratio is lowered when dopants are introduced (Table 1), this interesting behavior with PH$_3$ is attributed to a change in α_{vs}. Indeed, as one can see in Table 1, the $(b)^{1/2}\alpha_{vs}$ product remains essentially the same for the cases of GeH$_4$ and GeH$_4$/B$_2$H$_6$, and lower for the GeH$_4$/PH$_3$ case, suggesting a lower surface energy, α_{vs}, in the latter case after phosphine exposure and resulting in a lower d_c as observed experimentally (Figure 2e) and deduced from eq 2. This observation is in general agreement with incorporation of high concentrations of P into the NW sidewalls.[36] The excellent agreement between our experimental data and the model, both in integral (Figure 2a,c,d) and reduced form (Figure 2b,e), suggests that size effects in the growth of Ge NWs, and the suppression of growth at small diameters, are indeed governed by the Gibbs–Thomson effect.

However, after nearly five decades of NW growth by the widely used VLS mechanism, direct experimental validation of such assignment of an increase in equilibrium solute concentration with smaller diameters, and therefore reduc-

tion of supersaturation and NW growth rates has not been reported. Crucial for the detection and quantification of size effects is the use of linear arrays of NWs with a range of diameters, such as those shown in Figure 1b, which allow measurements on different-sized NWs under identical conditions (see Methods). For this purpose, in situ annealing experiments were performed on our ordered NW arrays in transmission electron microscopy (TEM).[37−39] By recording changes in the volume of the liquid Au−Ge alloy drops at the tips of solid NWs with varying temperature, the equilibrium composition of the nanoscale alloy (i.e., the liquidus of its binary phase diagram), was determined using a method described previously[40] and quantified for the first time here on different diameter NWs grown on the same substrate under identical conditions. We note that surface oxide layers that develop during sample transfer from the growth chamber to the TEM desorb at ~300 °C leaving a clean Ge NW surface exposed for these measurements.[37,40] The diameter-dependent Au−Ge alloy composition for selected NW diameters from an array similar to that in Figure 1b is shown in Figure 3. For all four temperatures considered, the equilibrium Ge atomic fraction shows a clear upward trend as the diameter decreases. The size-dependent Ge concentration is reproduced quantitatively by a thermodynamic relation based on the Gibbs−Thomson effect (see Supporting Information), $C_{NW} = C_\infty \exp(\kappa 4\Omega\alpha_{vs}/dkT)$. Using known values for C_∞, the temperature-dependent Ge concentration in a bulk Au−Ge alloy, fitted values for the factor κ, which accounts for changes in drop shape due to variations in the liquid, and liquid−solid surface and interface tensions with temperature,[41] we obtain the dashed curves in Figure 3 that show qualitatively agreement with the observed solute concentrations enhancement at small diameters.

The size-dependent equilibrium Ge content of Au−Ge alloy drops observed by TEM and the diameter-dependent
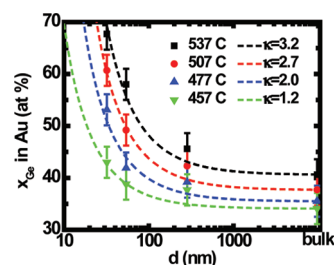
FIGURE 3. Ge atomic % as a function of diameter at different temperatures. Symbols are experimental data points; dashed lines are fits according to $C_{NW} = C_\infty \exp(\kappa 4\Omega\alpha_{vs}/dkT)$ (see text).

NW growth rate can be understood as related manifestations of the Gibbs−Thomson effect. The connection becomes evident in the following expression, which links the Ge concentration in the Au−Ge alloy drop, C_{NW}, to the supersaturation, $\Delta\mu$ (see Supporting Information):

$$\frac{\Delta\mu}{kT} = \frac{\Delta\mu_0}{kT} - \frac{1}{\kappa}\ln\left(\frac{C_{NW}}{C_\infty}\right) \qquad (4)$$

Equation 4 shows directly that a higher equilibrium Ge concentration, as observed by in situ TEM at higher temperature in Au−Ge alloy drops with smaller diameter, leads to a reduced supersaturation, that is, lower NW growth rate. For sufficiently small growth seeds with high Ge equilibrium concentration, the Ge supersaturation reduces to levels not sufficient for Ge NW growth, a thermodynamic effect that restricts the minimum achievable diameter in VLS growth. This result is in contrast to what has been postulated earlier about the nonexistence of such a limit[42] but in agreement with suggestions by others as to the critical condition for growth of small diameter Si NWs.[43]

The unified framework for size effects in NW growth provides the basis for understanding diameter-dependent growth rates and the lowest achievable diameter, the cutoff diameter d_c, of VLS-grown NWs. It also provides a useful basis for predicting the effects of different growth conditions on d_c. We now consider the role of temperature and GeH_4 partial pressure on growth rate and critical diameter. Our time dependent growth experiments have excluded incubation time effects as demonstrated in Figure 2 and Supporting Information Figures S5 and S6. In addition, we performed growth using the 366 °C nucleation temperature for 90 s only. For this and higher temperatures, the NW diameter is larger at the substrate interface and decreases gradually toward the NW tip due to moderate side-wall deposition through vapor−solid growth on the NW as shown in Figure 4a−d. The NW diameter for these growth temperatures is therefore measured at the NW tip near the Au nanoparticle to exclude diameter variation due to sidewall deposition. We emphasize here that the origin of tapering and subsequent diameter dependent-growth rate determination is fundamentally different from the cases of Si NW growth under conditions favoring Au diffusion and dynamic change in the seed particle size and NW diameter during growth; the latter case led to inconsistent size-dependent behavior in those studies.[15,16]

In our controlled experiments on Ge NW growth at elevated temperatures, we observe diameter-dependent growth rates, similar to those shown in Figure 2.[44] In particular, the data consistently show a linear dependence of $v^{1/2}$ on $1/d$ (Figure 2e). Hence, VLS NW growth at different temperatures can be understood within a common framework of the Gibbs−Thomson effect. The TEM experiments
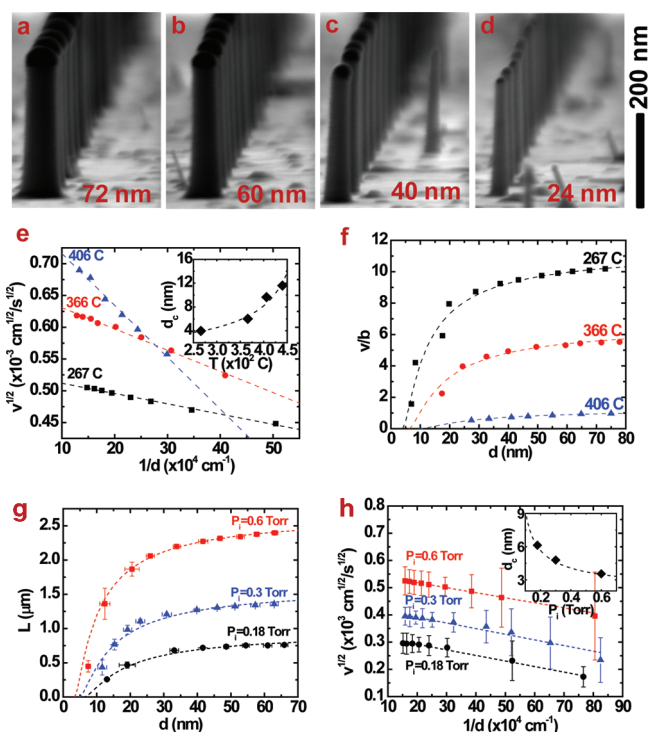
FIGURE 4. Dependence of growth rate and cutoff diameter on temperature and pressure. (a−d) SEM images of rows of Ge NWs after growth for 90 s at 366 °C for the indicated NW diameters. (e) Plot of $v^{1/2}$ as function of $1/d$ at different temperatures of 276, 366, and 406 °C showing different slopes and intercepts. Inset is a plot of the resulting critical diameter determined by the intercept as a function of temperature, illustrating higher cutoff diameters with higher temperatures. The dashed line in the inset is calculated according to eq 2. (f) Plot of the growth velocity normalized by the kinetic coefficient b for the data shown in (e). Solid symbols represent measured data and dashed lines represent calculations according to eq 3. (g) Plot of the NW length as function of diameter for different GeH_4 partial pressures for the two step growth conditions. (h) Plot of $v^{1/2}$ as a function of $1/d$ at different GeH_4 partial pressures for data of (g) showing the progressive reduction in the growth velocity with decreased diameter. Inset is a plot of the critical diameter as a function of input GeH_4 partial pressure showing logarithmic dependence and lower cutoff diameters with higher partial pressures. The dashed line in the inset is calculated according to eq 2, where $\Delta\mu_0$ has been obtained by a fit to the experimental data as function of $\ln|P_i|$.

have established that the equilibrium Ge concentration in Au−Ge alloys increases with temperature (Figure 3).[45] Thus we expect a reduced supersaturation, and consequently larger cutoff diameters, at higher growth temperatures. This behavior is indeed confirmed experimentally (Figure 4e). The resulting critical diameters, d_c, are plotted in the inset of Figure 4e as a function of temperature (see also Table 2). The observed increase in d_c with temperature is seen to agree well with the predictions from eq 2 as given by the dashed line in the inset. As illustrated in Figure 4f. v/b decreases with increased temperature and the cutoff diameter increases. It is the increase in the kinetic coefficient, b (see Table 2), that leads to the increase in the growth rate with temperature. Although not a focus of this present study, we also note that the nucleation efficiency for formation of

TABLE 2. Calculated Critical Diameters, Supersaturation Values, and Kinetic Coefficients Based on Measurements for Ge NWs Grown at 276, 366, 406, and 440 °C

T (°C)	d_c (nm)	$\Delta\mu_0$ (meV)	$\Delta\mu_0/kT$	b (10^{-8} cm/s)
276	3.4	145	3.1	3.0
366	6.0	82	1.5	20.5
406	9.7	51	0.9	80.5
440	11.6	43	0.7	86.9

a NW tends to decrease for diameters approaching d_c, and this effect is more pronounced at high temperatures.

One can also tune the Au–Ge supersaturation and thus the growth conditions by changing the input GeH$_4$ partial pressure. Thus, we have studied the effects of pressure on the Ge NW morphology and cutoff diameter. Figure 4g,h shows plots of the NW lengths and $v^{1/2}$ versus $1/d$ at different P_i[GeH$_4$] for our two step growth conditions. A lower P_i[GeH$_4$] results in reduced supersaturation and in d_c values of 3.6, 4.8, and 6.1 nm ($\pm$0.5 nm) for P_i[GeH$_4$] = 0.6, 0.3, and 0.18 Torr, respectively. This reduced supersaturation with decreasing pressure can be inferred from Figure 4h where the magnitude of the velocity decreases with decreasing P_i[GeH$_4$] while the slopes of these plots remain parallel, as was also noted by Givargizov for Si NW growth.[24] The parallel slopes suggest that the change in pressure has minimal effect on the kinetic coefficient b and the NW surface energy density α_{vs}.

A lower P_i[GeH$_4$] leads to less efficient nucleation for all NW diameters considered here and a higher P_i[GeH$_4$] results in enhanced NW tapering (see Supporting Information Figure S8). It is worth noting that plotting v versus $1/d$ according to Schmidt's et al. linear model[30] results in less accurate fits for all GeH$_4$ partial pressures than $v^{1/2}$ versus $1/d$, as shown in Supporting Information Figure S10, and in larger cutoff diameters of 6, 6.9, and 9 nm for P_i[GeH$_4$] = 0.6, 0.3, and 0.18 Torr. One can further explore the validity of the assumption of the square dependence versus the linear dependence of v as function of $\Delta\mu_0$ by growing Ge NWs at P_i[GeH$_4$] = 0.18 Torr and testing if any $\langle 111 \rangle$ wires can be grown below $d = 9$ nm, which is the cutoff diameter according to the linear dependence analysis. As shown in Supporting Information Figure S11, we observe Ge NWs as small as 6.5 nm diameter grown in the $\langle 111 \rangle$ orientation further supporting the use of the square dependence in our analysis. Since α_{vs} {111} < α_{vs} {100} < α_{vs} {110}[46] and since $\langle 110 \rangle$-oriented NWs have two-thirds {111} facets and one-third {100} facets, and $\langle 211 \rangle$ oriented NWs have two-fifths {111}, two-fifths {311}, and one-fifth {110} facets, one can deduce from eq 2 that these wire orientations will have lower cutoff diameters than the $\langle 111 \rangle$-oriented NWs with {211} surface facets. Both types of wires with diameters less than 9 nm have indeed been observed in our P_i[GeH$_4$] = 0.18 Torr experiments as shown in Supporting Information Figure S12.

Our analysis of size effects in the synthesis of Ge NWs provides the first direct and quantitative validation of a thermodynamic limit on the achievable NW diameter in VLS growth by combining observations of the reduced growth rate and enhanced equilibrium Ge solubility in the liquid Au–Ge growth seeds. The unified framework for understanding these nanoscale size effects, based on the Gibbs–Thomson effect, provides a basis for analyzing the cutoff diameter and other size-dependent growth phenomena at small diameters for a wide variety of other semiconductor materials that form NWs by the VLS process. Aside from conventional growth parameters, such as temperature or precursor pressure, surface energies are a key factor in synthesis processes at the nanoscale. For example, the manipulation of the vapor-surface energy of the NW side facets by dopants or surfactants can enable the cutoff diameter of VLS NWs to be tuned, thus extending diameters close to the atomic scale. Because of their differences in surface energies, atomic volumes, and supersaturations, Si NWs should grow to about 60% smaller diameter than Ge,[11,47] and changes in growth orientation, that is, in the exposed facets, will influence the minimum diameter. The prospect of controlling the synthesis of semiconductor NWs at extremely small diameters paves the way for the fabrication of one-dimensional nanomaterials with strong carrier confinement and energy quantization. Calculations suggest for instance that the electronic properties of [111]-oriented Ge NWs will change from indirect to direct band gap below 10 nm,[48] possibly providing significant enhancements in light absorption and emission. Ultrathin NWs may show carrier multiplication, so far observed only in nanoparticles,[49] and would facilitate the extraction of such additional charges, that is, may allow realizing the resulting performance gains in solar cell and sensor applications.

Methods. Ge (111) surfaces were prepared by organic solvent cleaning, deionized water (DI) rinse, buffered oxide etch dip followed by DI rinse, and N$_2$ blow dry. For the case of Au colloids dispersed from solution, citrate-stabilized Au colloids that are commercially available (Ted Pella) were used. The solutions were diluted in isopropanol (IPA) and transferred onto 3-aminopropyldiethoxysilane-treated Ge(111) surfaces. For the case of e-beam lithography patterned Au dots and patterned small areas of Au films used as alignment marks, ~230 nm of PMMA C 3% was spun cast on the Ge(111) surfaces and exposed using a JEOL JBX-6300FS e-beam writer to pattern Au dots with diameters in the range of 30–100 nm. Following development in methyl-isobutyl-ketone (MIBK)–IPA, the Ge samples were loaded into an electron beam evaporator and 20 nm of Au was evaporated. The Au layer was then lifted-off in acetone assisted by a brief sonication. Prior to loading the samples into the growth reactor, another sequence of solvent cleaning was performed and the samples were treated with UV ozone for 5 min. This procedure minimized the nucleation of stray wires in between the arrays.

Ge NW growth was performed in a cold wall CVD system (Atomate Inc.). The temperature was ramped gradually to 125 °C and held there for ~10 min followed by a ramp to the nucleation or growth temperature. For two-step growth,

the temperature was ramped to 366 °C where 250 sccm GeH$_4$ (30 % in H$_2$) was introduced for 1.5 min to nucleate the Ge NWs at 2 Torr chamber pressure. The growth temperature was then ramped down to 276 °C in 3 min while maintaining constant GeH$_4$ flow and chamber pressure. NW elongation then proceeded for the desired time (15 min for the growth from colloidal Au nanoparticles and 10 min for the growth from e-beam patterned Au dots). For the doped wires, 100 sccm of PH$_3$, or 50 sccm of B$_2$H$_6$ (both at 100 ppm in H$_2$) were flown into the reactor along with the 250 sccm of GeH$_4$ at a constant chamber pressure of 2 Torr. Single step constant temperature growth was also carried out at 366, 406, and 440 °C with P_i[GeH$_4$] = 0.6 Torr. Several pressures for the two-step growths (366−276 °C) were performed with P_i[GeH$_4$] = 0.6, 0.3, and 0.18 Torr. Post growth, the NW dimensions were measured and imaged in an FEI X30 environmental scanning electron microscope. The lithographically defined Au dots and films were used for all the growth rate data shown in this work. The TEM variable temperature experiments were performed in a JEOL JEM 3000F field emission TEM equipped with a Gatan 652 high-temperature sample holder (see ref 40).

Supporting Information Available. Experimental details, relationship between Ge concentration in the Au−Ge VLS seed drop and the supersaturation, $\Delta\mu$, driving Ge nanowire growth, and additional references. This material is available free of charge via the Internet at http://pubs.acs.org.

REFERENCES AND NOTES

(1) Wagner, R. S.; Ellis, W. C. Vapor−Liquid−Solid Mechanism of Single Crystal Growth. *Appl. Phys. Lett.* **1964**, *4*, 89.

(2) Morales, A. M.; Lieber, C. M. A Laser Ablation Method for the Synthesis of Crystalline Semiconductor Nanowires. *Science* **1998**, *279*, 5348.

(3) Adhikari, H.; Marshall, A. F.; Goldthorpe, I. A.; Chidsey, C. E. D.; McIntyre, P. C. Metastability of Au-Ge Liquid Nanocatalysts: Ge Vapor−Liquid−Solid Nanowire Growth Far below the Bulk Eutectic Temperature. *ACS Nano* **2007**, *1*, 415.

(4) Dayeh, S. A.; Yu, E. T.; Wang, D. III-V Nanowire Growth Mechanism: V/III Ratio and Temperature Effects. *Nano Lett.* **2007**, *7*, 2486.

(5) Borgstrom, M. T.; Immink, G.; Ketelaars, B.; Algara, R.; Bakkers, E. P. A. M. Synergetic Nanowire Growth. *Nat. Nanotechnol.* **2007**, *2*, 541.

(6) Dayeh, S. A.; Yu, E. T.; Wang, D. Surface Diffusion and Substrate-Nanowire Adatom Exchange in InAs Nanowire Growth. *Nano Lett.* **2009**, *9*, 1967.

(7) Carim, A. H.; Lew, K. K.; Redwing, J. M. Bicrystalline Silicon Nanowires. *Adv. Mater.* **2001**, *13*, 1489.

(8) Kamins, T. I.; Li, X.; Williams, R. S. Growth and Structure of Chemically Vapor Deposited Ge Nanowires on Si Substrates. *Nano Lett.* **2004**, *4*, 503.

(9) Givargizov, E. I. Fundamental Aspects of VLS Growth. *J. Cryst. Growth* **1975**, *31*, 20.

(10) Wu, Y.; Fan, R.; Yang, P. Block-by-Block Growth of Single-Crystalline Si/SiGe Superlattice Nanowires. *Nano Lett.* **2002**, *2*, 83.

(11) Zhang, X.; Lew, K.-K.; Nimatoori, P.; Redwing, J. M.; Dickey, C. Diameter-Dependent Composition of Vapor−Liquid−Solid Grown Si$_{1-x}$Ge$_x$ Nanowires. *Nano Lett.* **2007**, *7*, 3241.

(12) Clark, T. E.; Nimmatoori, P.; Lew, K.-K.; Pan, L.; Redwing, J. M.; Dickey, E. C. Diameter Dependent Growth Rate and Interfacial Abruptness in Vapor−Liquid−Solid Si/Si$_{1-x}$/Ge$_x$ Heterostructure Nanowires. *Nano Lett.* **2008**, *8*, 1246.

(13) Schmid, H.; Bjork, M. T.; Knoch, J.; Karg, S.; Riel, H.; Riess, W. Doping Limits of Grown in situ Doped Silicon Nanowires Using Phosphine. *Nano Lett.* **2009**, *9*, 173.

(14) Weyher, J. Some Notes on the Growth Kinetics and Morphology of VLS Silicon Crystals Grown with Platinum and Gold as Liquid-Forming Agents. *J. Cryst. Growth* **1978**, *43*, 235.

(15) Kodambaka, S.; Tersoff, J.; Reuter, M. C.; Ross, F. M. Diameter-Independent Kinetics in the Vapor−Liquid−Solid Growth of Si Nanowires. *Phys. Rev. Lett.* **2006**, *96*, No. 096105.

(16) Schmid, H.; Bjork, M. T.; Knoch, J.; Riel, H.; Riess, W. Patterned Epitaxial Vapor−Liquid−Solid Growth of Silicon Nanowires on Si(111) Using Silane. *J. App. Phys.* **2008**, *103*, No. 024304.

(17) Sierra-Sastre, Y.; Dayeh, S. A.; Picraux, S. T.; Batt, C. A. Epitaxy of Ge Nanowires From Biotemplated Au Nanoparticle Catalysts. *ACS Nano* **2010**, *4*, 1209.

(18) Sze, S. M., Ng, K. K. Physics of Semiconductor Devices, 3rd ed.; Wiley-Interscience: New York, 2007.

(19) Wang, D.; Wang, Q.; Javey, A.; Tu, R.; Dai, H.; Kim, H.; McIntyre, P. C.; Krishnamohan, T.; Saraswat, K. C. Germanium Nanowire Field-Effect Transistors with SiO$_2$ and high-k HfO$_2$ gate dielectrics. *Appl. Phys. Lett.* **2003**, *83*, 2432.

(20) The temperature was calibrated using an ∼1 × 1 cm^2 cut from a 2 in. KLA Sensor model 1530A-2, which is 4 times the size of the samples used in our growths (0.5 × 0.5 cm^2). A K-type sensor was mounted on the surface a 1 mm thick Si sample. The Ge samples used in our growths were 0.7 mm thick.

(21) Dhalluin, F.; Baron, T.; Ferret, P.; Salem, B.; Gentile, P.; Harmand, J.-C. Silicon Nanowires: Diameter Dependence of Growth Rate and Delay in Growth. *Appl. Phys. Lett.* **2010**, *96*, 133109.

(22) Warnock, J.; Awshalom, D. D.; Schafer, M. W. Geometrical Supercooling of Liquids in Porous Glasses. *Phys. Rev. Lett.* **1986**, *57*, 1753.

(23) Ostwald, W. *Lehrbuch der Allgemeinen Chemie*; Engelmann: Leipzig, Germany, 1896; Vol. 2, part 1.

(24) Givargizov, E. I. *Highly Anisotropic Crystals*. Springer: New York, 1987; Chapter 2, pp 100−112.

(25) Givargizov, E. I.; Chernov, A. A. Rate of Whisker Growth by the Vapor−Liquid−Crystal Mechanism and the Role of Surface Energy. *Kristallografiya* **1973**, *18*, 147.

(26) Dubrovskii, V. G.; Sibirev, N. V. Growth Rate of a Crystal Facet of arbitrary Size and Growth Kinetics of Vertical Nanowires. *Phys. Rev. E* **2004**, *70*, No. 031604.

(27) Dubrovskii, V. G.; Cirlin, G. E.; Soshnikov, I. P.; Tonkikh, A. A.; Sibirev, N. V.; Samsonenko, Y. B.; Ustinov, V. M. Diffusion Induced Growth of GaAs Nanowhiskers During Molecular Beam Epitaxy: Theory and Experiment. *Phys. Rev. B* **2005**, *71*, 205325.

(28) Kashchiev, D. Dependence of the Growth Rate of Nanowires on the Nanowire Diameter. *Cryst. Growth Design* **2006**, *6*, 1154.

(29) Dubrovskii, V. G.; Sibirev, N. V. General Form of the Dependence of Nanoiwre Growth Rate on the Nanowire Radius. *J. Cryst. Growth* **2007**, *304*, 504.

(30) Schmidt, V.; Senz, S.; Gosele, U. Diameter Dependence of the Growth Velocity of Silicon Nanowires Synthesized via the Vapor−Liquid−Solid Mechanism. *Phys. Rev. B* **2007**, *75*, No. 045335.

(31) Dubrovskii, V. G.; Sibirev, N. V.; Cirlin, G. E.; Soshnikov, I. P.; Chen, W. H.; Larde, R.; Cadel, E.; Pareige, P.; Xu, T.; Grandidier, B.; Nys, J.-P.; Stievenard, D.; Moewe, M.; Chuang, L. S.; Chang-

Hasnain, C. Gibbs-Thomson and Diffusion-Induced Contributions to the Growth Rate of Si, InP, and GaAs Nanowires. *Phys. Rev. B* **2009**, *79*, 205316.

(32) Schmidt, V.; Wittemann, J. V.; Senz, S.; Gosele, U. Silicon Nanowires: A Review on Aspects of their Growth and their Electrical Properties. *Adv. Mater.* **2009**, *21*, 2681.

(33) We have used a Ge atomic volume of $\Omega = 2.26 \times 10^{-23}$ cm^{-3}, and α_{vs} Ge (110) facets of 0.88×10^{-4} J/cm^{-2} according to Jiang, Q.; Lu, H. M.; Zhao, M. Modelling of Surface Energies of Elemental Crystals. *J. Phys.: Condens. Matter* **2004**, *16*, 521.

(34) Four-probe measurements on separate wires grown under similar doping conditions and assuming bulk electron mobility values lead to an estimate of $\sim 10^{18}$ cm^{-3} n-type phosphorous doping. p-type boron VLS doping is expected to be within the same range but has not been experimentally evaluated by us.

(35) $\Delta\mu_0$ is also a function of temperature and pressure. A lower temperature and higher pressure will lead to an increased $\Delta\mu_0$ and therefore reduced critical diameters. However, the lower temperature cannot be too much lower than the eutectic temperature for efficient VLS growth, and therefore, we have a lower limit at which we can reduce the temperature and still grow NWs. On the other hand, a higher pressure will lead to enhanced side-wall deposition and tapering in the NWs as shown in Supporting Information Figure S7 and therefore, there are also practical limits on how high a pressure we can use.

(36) Perea, E.; Hemesath, E. R.; Schwalbach, E. J.; Lensch-Falk, J. L.; Voorhees, P. W. Direct Measurement of Dopant Distribution in an Individual Vapour−Liquid−Solid Nanowire. *Nat. Nanotech.* **2009**, *4*, 315.

(37) Sutter, E.; Sutter, P. Au-Induced Encapsulation of Ge Nanowires in Protective Shells. *Adv. Mater.* **2006**, *18*, 2583.

(38) Kodambaka, S.; Tersoff, J.; Reuter, M. C.; Ross, F. M. Germanium Nanowire Growth Below the Eutectic Temperature. *Science* **2007**, *316*, 729.

(39) Kim, B. J.; Tersoff, J.; Kodambaka, S.; Reuter, M. C.; Stach, E. A.; Ross, F. M. Kinetics of Individual Nucleation Events Observed in Nanoscale Vapor−Liquid−Solid Growth. *Science* **2008**, *322*, 1070.

(40) Sutter, E.; Sutter, P. Phase Diagram of Nanoscale Alloy Particles Used for Vapor−Liquid−Solid Growth of Semiconductor Nanowires. *Nano Lett.* **2008**, *8*, 411.

(41) Naidich, Y. V.; Perevertailo, V. M.; Obushchak, L. P. Contact Properties of the Phases Participating in the Crystallization of Gold-Silicon and Gold-Germanium Melts. *Poroshkovaya Metallurgia* **1975**, *151*, 63.

(42) Tan, T. Y.; Li, N.; Gosele, U. Is There as Thermodynamic Size Limit of Nanowires Grown by the Vapor−Liquid−Solid Process. *Appl. Phys. Lett.,* **2007**, *183*, 1199.

(43) Dhalluin, F.; Desre, P. J.; den Hertog, M. I.; Rouviere, J.-L.; Ferret, P.; Gentile, P.; Baron, T. Critical Condition for Growth of Silicon Nanowires. *J. Appl. Phys.* **2007**, *102*, No. 094906.

(44) Growth at 366, 406, and 440 °C was performed as a single temperature procedure, but otherwise similar conditions to those discussed in Figure 1b−j, since Ge NW nucleation occurs readily above the eutectic temperature. The observations of diameter dependent growth behavior are consistent for the single temperature step and two temperature step growth procedures.

(45) The same trend is predicted by Supporting Information eq S2, dominated by the temperature dependence of C_∞ rather than the $1/T$ term in the exponential.

(46) Hanrath, T.; Korgel, B. A. Crystallography and Surface Faceting of Germanium Nanowires. *Small* **2005**, *1*, 717.

(47) Wu, Y.; Cui, Y.; Huynh, L.; Barrelet, C. J.; Bell, C. B.; Lieber, C. M. Controlled Growth and Structures of Molecular-Scale Silicon Nanowires. *Nano Lett.* **2004**, *4*, 433.

(48) Jing, M.; Ni, N.; Song, W.; Lu, J.; Gao, Z.; Lai, L.; Mei, W. N.; Yu, D.; Ye, H.; Wang, L. Anisotropic and passivation-dependent quantum confinement effects in germanium nanowires: a comparison with silicon nanowires. *J. Phys. Chem. B* **2006**, *110*, 18332.

(49) Klimov, V. I. Mechanisms for photogeneration and recombination of multiexcitons in semiconductor nanocrystals: implications for lasing and solar energy conversion. *J. Phys. Chem. B* **2006**, *110*, 16827.

Supplementary Information:

Direct Observation of Nanoscale Size Effects in Ge Semiconductor Nanowire Growth

Shadi A. Dayeh, and S. T. Picraux[*]

Center for Integrated Nanotechnologies (CINT), Los Alamos National Laboratory

*To whom correspondence should be addressed, STP picraux@lanl.gov or SAD shadi@lanl.gov.

Supporting information

1. Experimental Details

2. Relationship between Ge concentration in the Au-Ge VLS seed drop and the supersaturation, $\Delta\mu$, driving Ge nanowire growth

3. References

1. Experimental Details
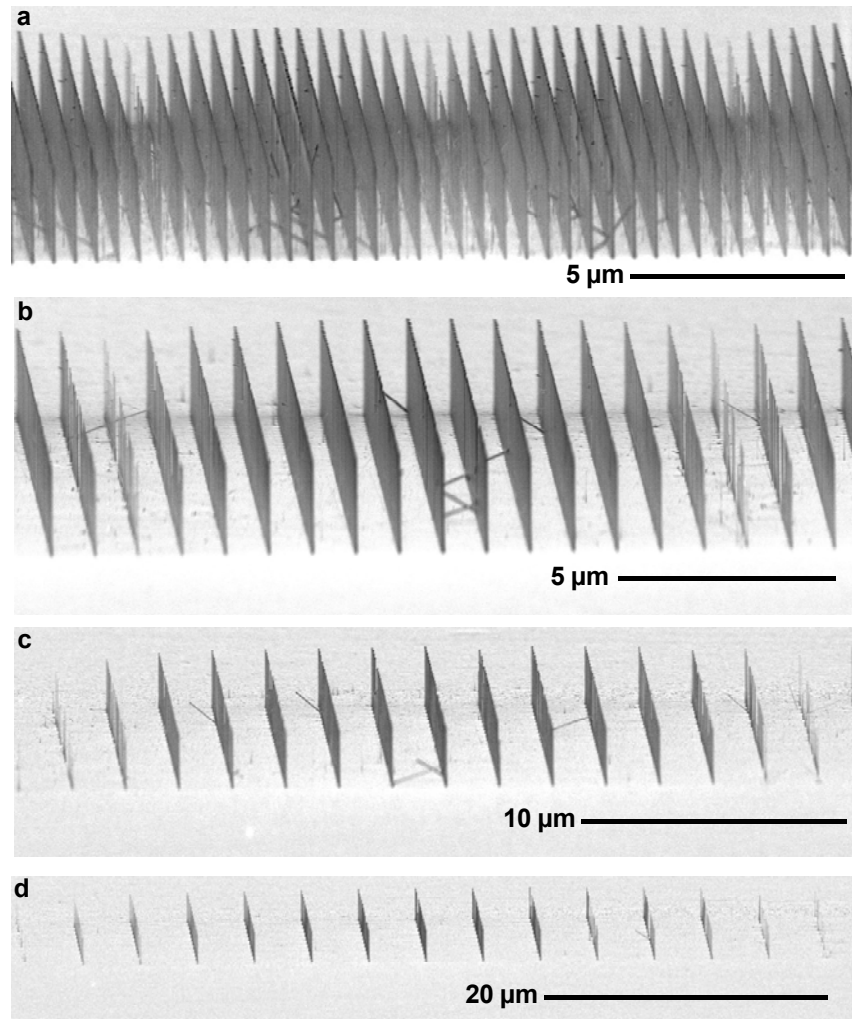
Figure S1 Ge nanowire growth for different diameters and inter-wire spacings. Oblique (80° viewing angle) field-emission scanning electron microscopy (FE-SEM) images of ordered arrays of NWs grown by two-step growth (see Methods) from 20 nm thick Au discs with diameter changing between 30 nm (shortest NWs) and 100 nm (longest NWs) in 10 nm steps along the horizontal direction. Inter-wire spacing in both x and y directions are: **a** 0.5 µm; **b** 1 µm; **c** 2 µm; **d** 4 µm. The Ge <111> oriented vertical NW diameter-dependent growth rate is observed to be independent of inter-wire spacing.
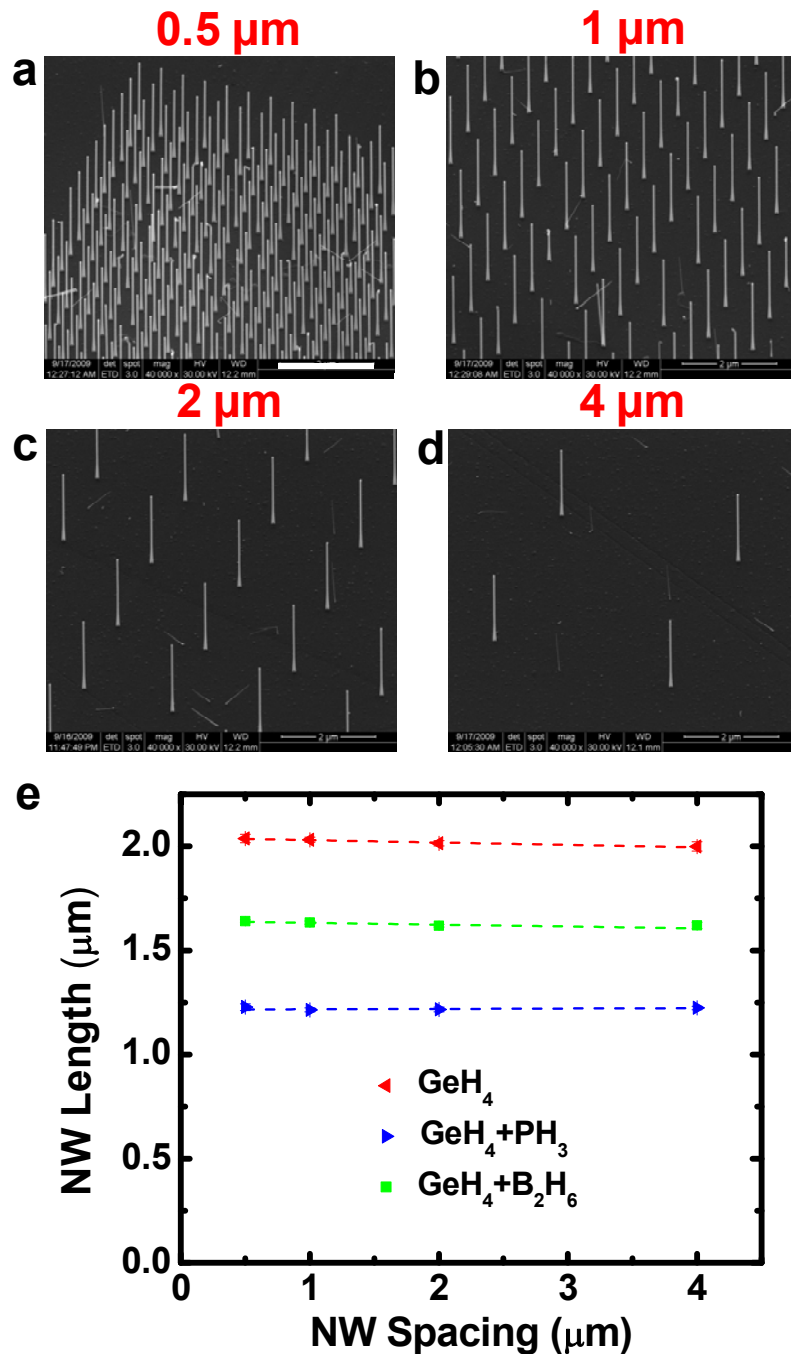
Figure S2 Ge nanowire growth rate does not depend on inter-wire spacing.
a– d 45º viewing angle FE-SEM images of undoped Ge NWs grown by two-step growth (see Methods) from 40 nm diameter and 20 nm thick Au discs with 0.5 µm, 1 µm, 2 µm, and 4 µm inter-spacing. Scale bar: 2 µm. **e** Plot of the NW growth rate as function of inter-wire spacing for undoped, P-doped n-type, and B-doped p-type. The NW length for fixed diameter (40 nm) is observed to be independent of spacing, demonstrating the absence of synergetic effects or adjacent NW interaction.
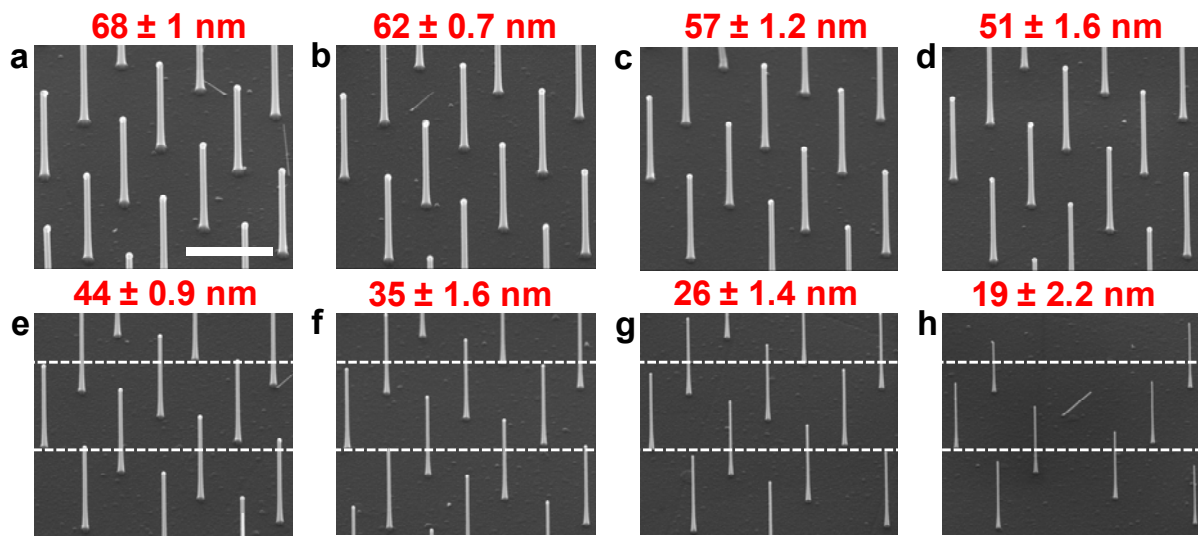
Figure S3 Diameter-dependent growth rate of Ge nanowires n-doped by PH₃.
a – h 45° angle view SEM micrographs of nanowires grown from 100, 90, 80, 70, 60, 50, 40, and 30 nm diameter Au discs of 20 nm thickness by two-step growth (see Methods) with 1 μm inter-spacing. The growth (elongation time) time is 10 minutes at 276 ºC with a germane partial pressure of $P_i[GeH_4]$=0.43 Torr and phosphine partial pressure of $P_i[PH_3]$=57.1 μTorr. The resultant NW diameter and its standard deviation in the array are indicated at the top of each SEM image. Scale bar: 1 μm. Dashed lines on images **e – h** highlight the reduced nanowire length at smaller Au diameters.
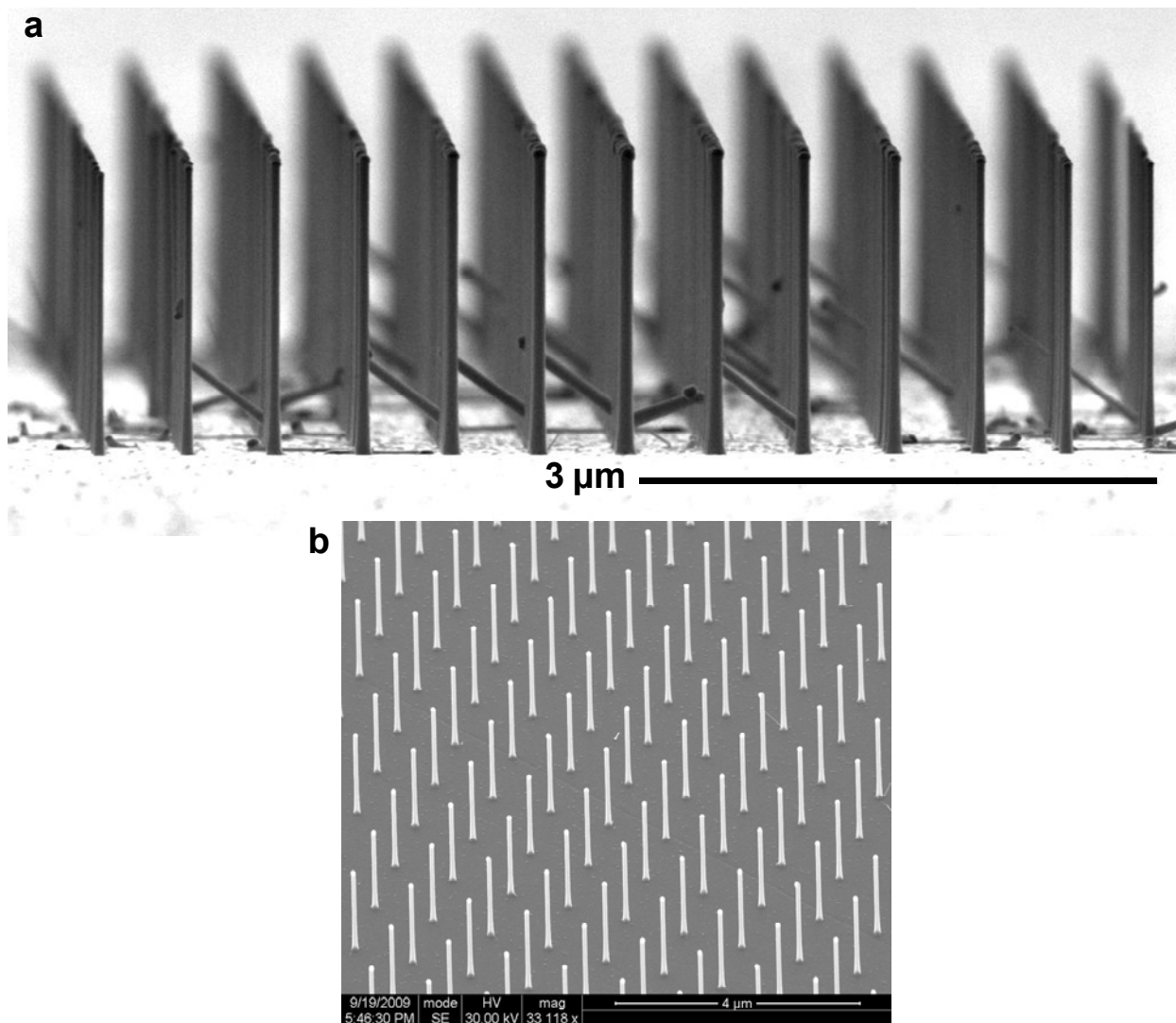
Figure S4 Diameter-dependent growth rate of Ge nanowires p-doped by B_2H_6.
a ~ 89 deg FE-SEM image of Ge NWs grown from 100, 90, 80, 70, 60, 50, 40, and 30 nm diameter Au discs of 20 nm thickness by two-step growth (see Methods) with 0.5 μm inter-spacing. The growth (elongation time) time is 10 minutes at 276 ºC with P[GeH_4]=0.43 Torr and P[B_2H_6]=33.3 μTorr. NW lengths are observed to be reduced at smaller Au diameters. **b** 45° angle view of an ordered arrays of Ge NWs grown from 90 nm diameter dots with 1 μm inter-wire spacing. High efficient nucleation and uniform, highly vertical growth is observed for these conditions.
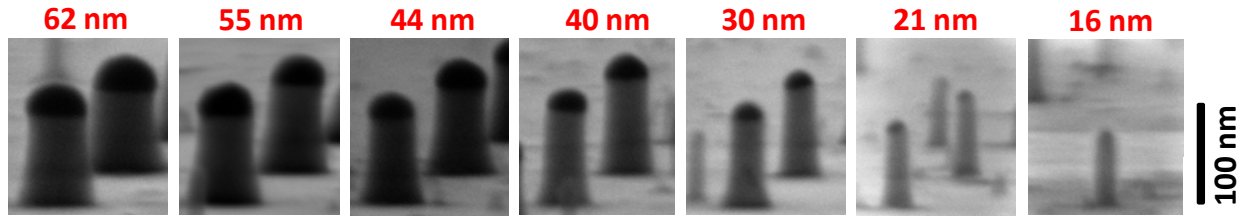
Figure S5 Initial nanowire growth at very short nucleation/incubation times.
SEM micrographs of Ge NWs grown at 366ºC for 30 sec at germane partial pressure $P_i[GeH_4]=$ 0.6 Torr for various diameter Au dots. NW diameters taken just below the Au are given above each figure. These images were taken from e-beam lithography patterned Au dots. No apparent nucleation/incubation effects were observed over this time scale which is much shorter than the time scales we use for all the other growths discussed in this work. The smallest diameter colloids still grew shorter NWs, indicating efficient nucleation and that incubation effects at short times did influence the growth rate measurements.
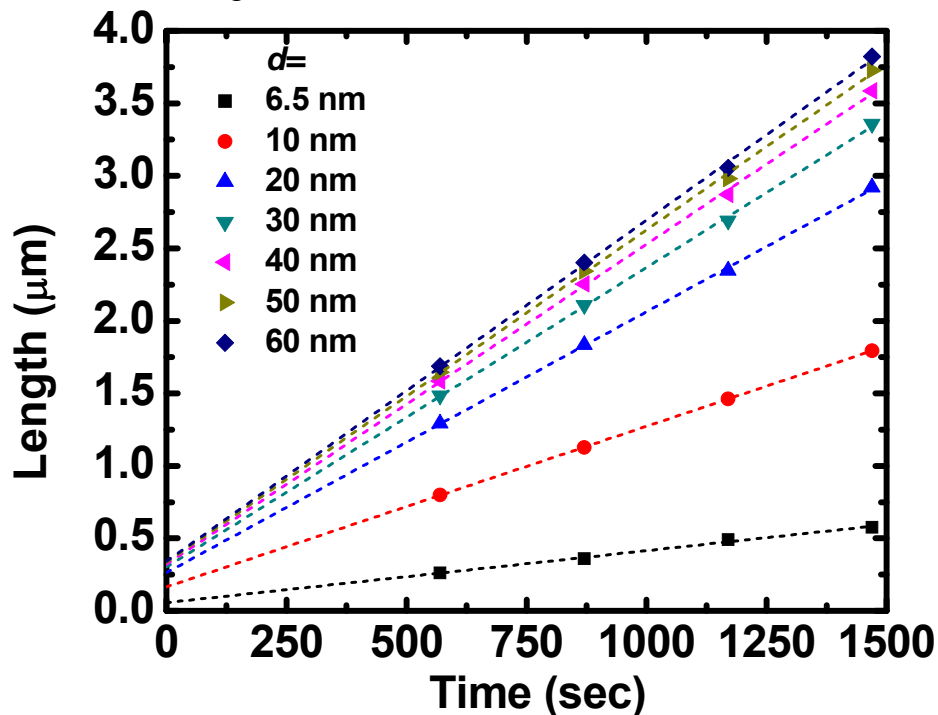
Figure S6 Linear growth rate with time is observed.
Ge NW length is plotted as a function of growth time, extracted from Fig. 2a grown in a germane partial pressure $P_i[GeH_4]=0.6$ Torr. A linear growth rate is observed with growth time. The non-zero intercept is due to the 2-step temperature process where the growth is somewhat faster during the nucleation step (366 °C for 90 sec) and then becomes constant at the elongation temperature (276 °C, for t $\geq$ 5 min).
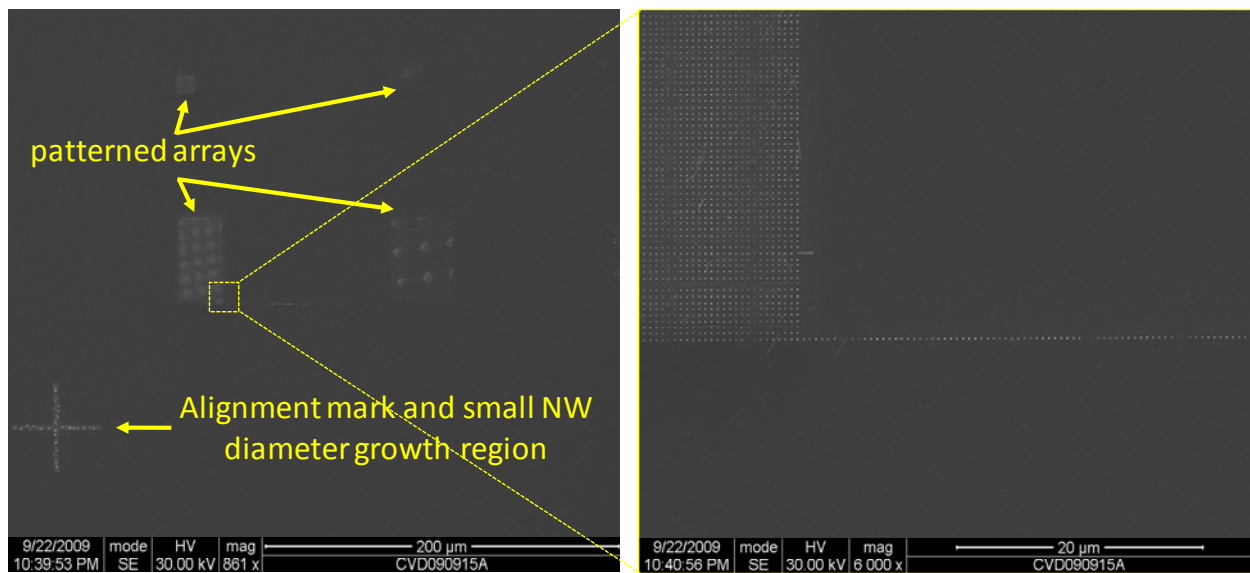
Figure S7 Large area map of NW growth from patterned Au on Ge(111) surfaces.
SEM images showing the location of the lithographically patterned Au dot arrays and larger area Au films used for cross alignment marks (present at 4 corners of pattern) used to locate the patterns. Smaller diameter NWs could be grown from the Au films than could be achieved with the patterned Au dots. All growth is performed simultaneously for the two regions.
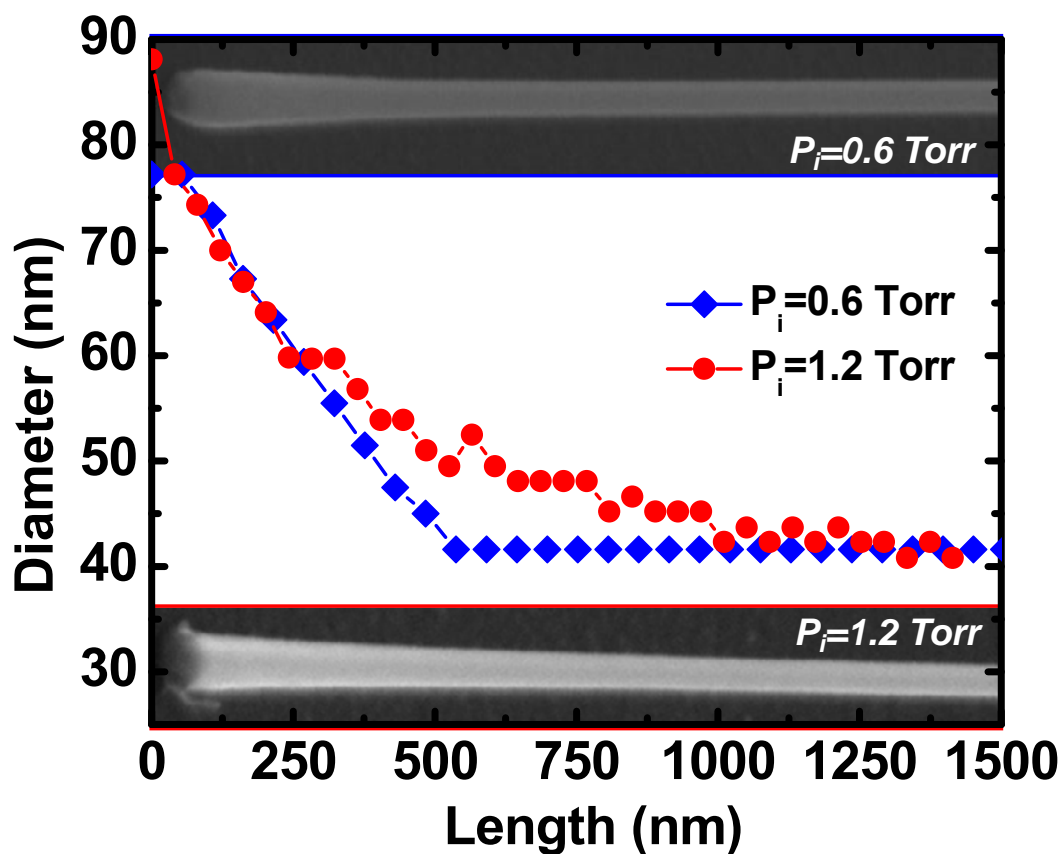
Figure S8 Nanowire tapering at higher pressures.
Plot of NW diameter as function of length for 2 NWs grown from 40 nm Au colloids at $P_i[GeH_4]$=0.6 Torr (typically used in our experiments) and $P_i[GeH_4]$ =1.2 Torr. The higher pressure results in enhanced side-wall deposition and tapering of the NW.
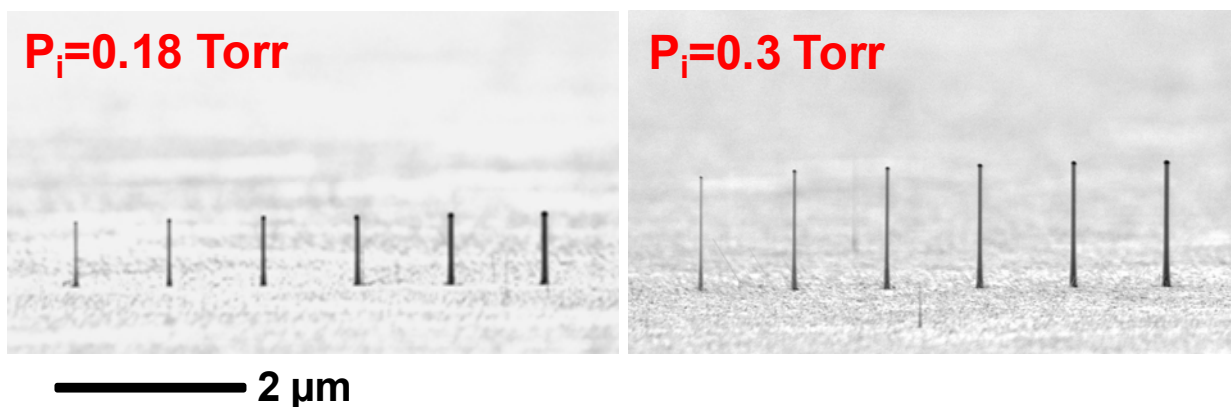
Figure S9 Pressure dependence of nanowire growth rate.

SEM images of Ge NW arrays grown at different $P_i[GeH_4]$ as indicated in the figures. The growth was by the two-step growth process at 276ºC for 10 min. elongation time from lithographically patterned Au discs of thickness 20 nm and diameters (left to right) 33, 42, 49, 54, 61, and 66 nm. Results demonstrate NW growth rate increases with pressure.
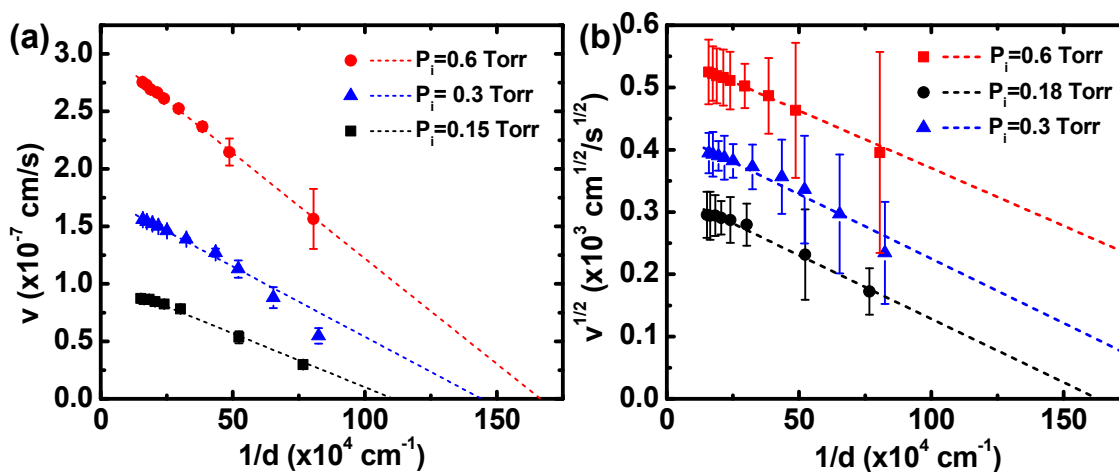
Figure S10 Growth kinetics comparison.

Comparison between the linear (a) and square (b) dependence of growth velocity on supersaturation (1/d) for Ge NWs grown by the two-step growth process at 276ºC for 10 min. elongation time at the three indicated germane partial pressures. Intercepts with abscissa give predicted cutoff diameters for growth.

(a) d=6.5 nm

(b) <111> <022>
5 1/nm

(c) d=9.5 nm

(d) <111>
2 1/nm

(e) d=13 nm

(f) <111>
2 1/nm
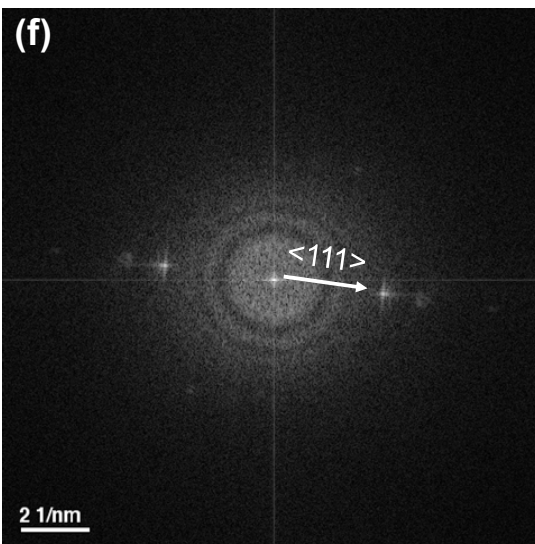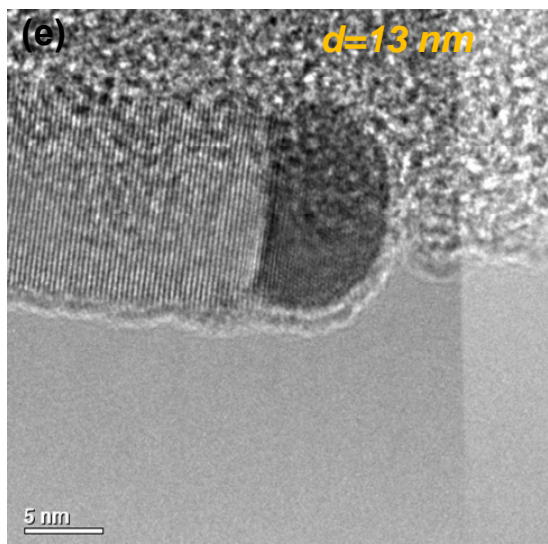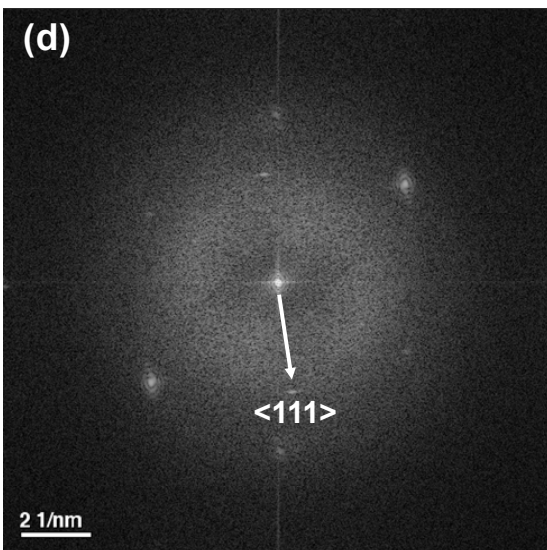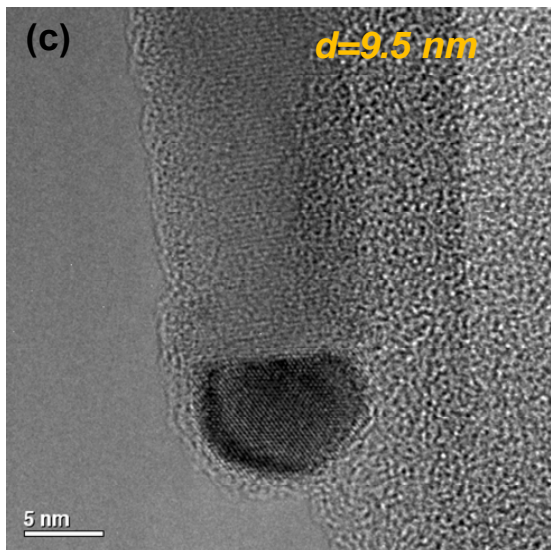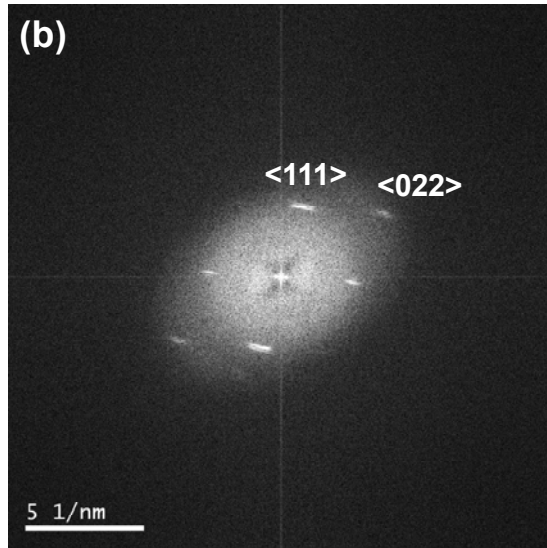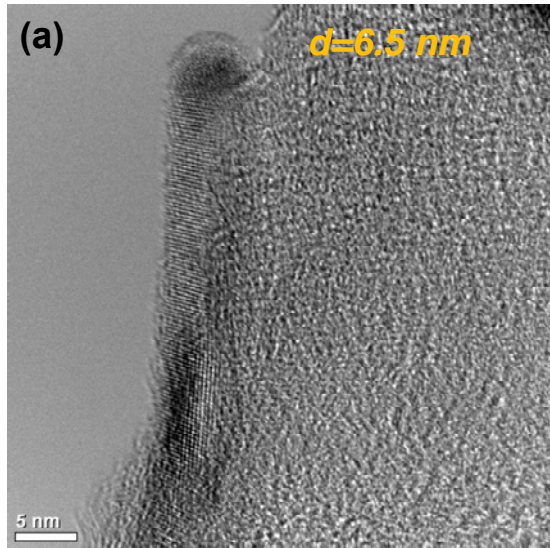
Figure S11 Ge <111> oriented nanowire growth at small diameters.
(**a,c,e**) HRTEM images and (**b,d,f**) FFT pattern of a (**a,b**) 6.5 nm, (**c,d**) 9.5 nm, and (**e,f**) 13 nm diameter <111> oriented Ge NW grown at $P_i[GeH_4]$=0.18 Torr by the two-step growth process at 276ºC for 10 min elongation time. These nanowires are grown from Au colloids. The spreading in the FFT spots in (**b**) is due to bending of the 6.5 nm diameter Ge NW; the small NWs tend to be attracted to the edge of the lacey carbon film.
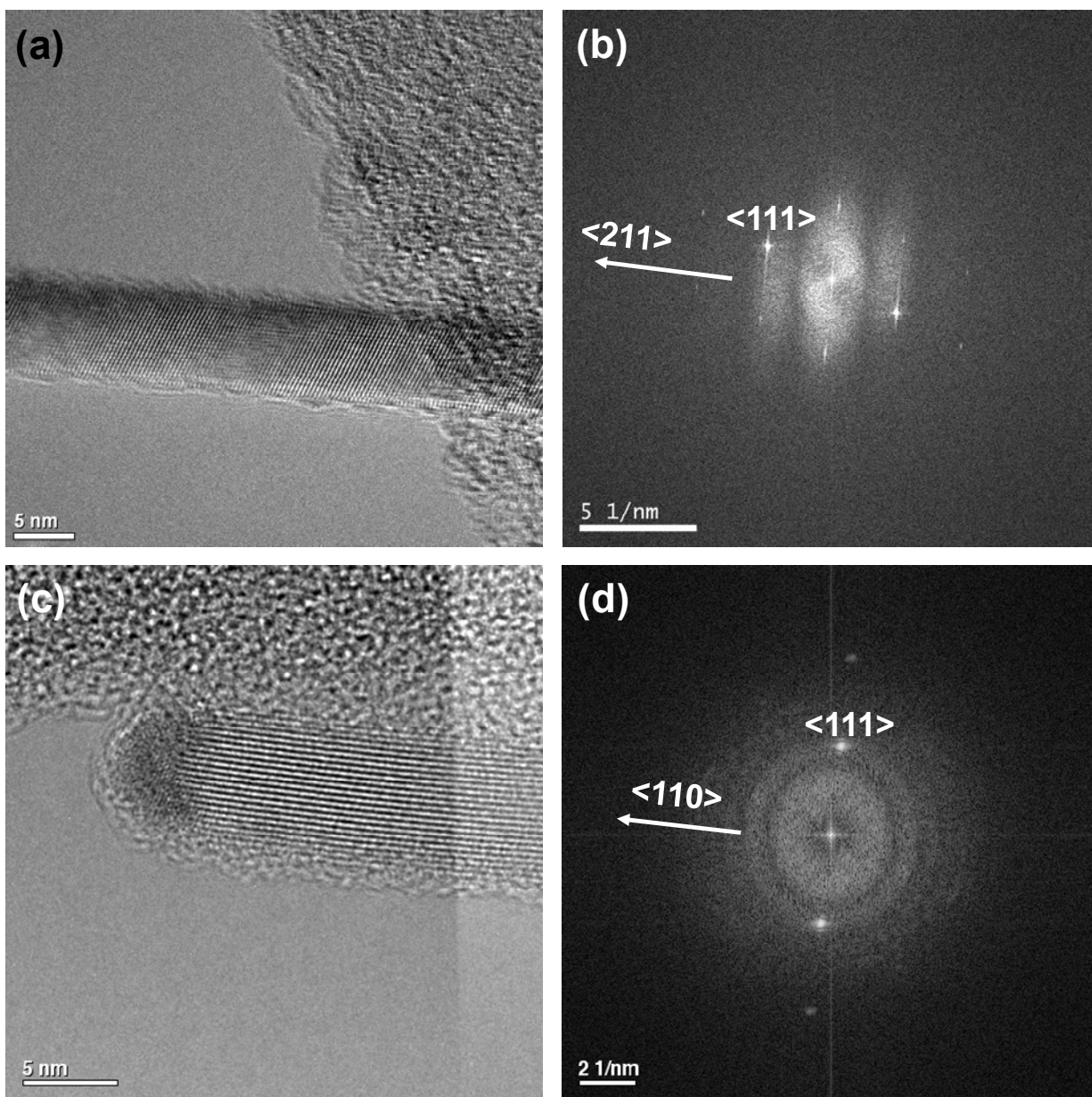
Figure S12 Ge <211> and <110> oriented nanowires are also observed to grow at small diameters. HRTEM images and FFT patterns of (**a-b**) 8.4 nm <211> oriented and (**c-d**) 7 nm diameter <110> oriented Ge NW grown under the same conditions as for Figure S10.

2. Relationship between Ge concentration in the Au-Ge VLS seed droplet and the supersaturation Δμ driving Ge nanowire growth

The diameter-dependent vapor pressure of solute in a Au nanoparticle, $P_{NW}(d)$, can be expressed as a function of its vapor pressure in bulk Au, P_∞, as follows [1]:

$$P_{NW}(d) = P_\infty \exp\left(4\Omega\alpha_{lv} / dkT\right) \approx P_\infty \exp\left(4\kappa\Omega\alpha_{vs} / dkT\right). \qquad (S1)$$

In the temperature range used in our experiments, $\alpha_{lv} \approx \alpha_{vs}$ ($\alpha_{lv} \sim 0.78$ J/m^2 and 0.8 J/m^2 for temperatures of 404°C and 470 °C, respectively, which is similar to the (110) Ge surface energy density of 0.88 J/m^2 [2]). This difference in α_{lv}, α_{vs} is typically neglected in the literature[3]. The term κ is added to equation S1 to take into account surface energy density changes, and consequently curvature changes with temperature, as described below.

The equilibrium geometry of a liquid droplet at the tip of a NW is determined by a balance of forces, described by a reduced modified Young's equation, $\cos\beta \approx -\alpha_{ls} / \alpha_{lv}$, where β is the contact angle at the solid-liquid interface [4]. For macroscopic Au-Ge drops on extended planar Ge surfaces, the contact angle β decreases with increasing temperature along the (bulk) liquidus [5]. This results from a more rapid decrease in α_{ls} with temperature than α_{lv}, as can be inferred from the reduced modified Young's equation or as quantified in ref. [5]. The contact angles observed between our nanoscale Au-Ge droplets and Ge NWs show the same behavior, i.e., become progressively smaller at higher temperatures. Using equation S1 and Henry's law, $P_i = \kappa C_i$, where κ is a temperature dependent constant and C_i denotes the concentration of component i of a solution, one can express the Ge concentration in the Au-Ge alloy, C_{NW}, as

$$C_{NW} = C_\infty \exp\left(\kappa 4\Omega\alpha_{vs} / dkT\right), \qquad (S2)$$

where C_∞ is the temperature-dependent Ge concentration in a bulk Au-Ge alloy. With the aid of equation (S2), equation (1) can be re-written as

$$\frac{\Delta\mu}{kT} = \frac{\Delta\mu_0}{kT} - \frac{1}{\kappa}\ln\left(\frac{C_{NW}}{C_\infty}\right).$$

(S3)

Equation (S3) shows directly that higher equilibrium Ge concentration in Au-Ge alloy droplets with smaller diameter, as observed in high-temperature in situ TEM (Figure 3), leads to a reduced supersaturation, i.e., a lower nanowire growth rate. We refer to this size-dependent supersaturation (or equivalently higher equilibrium Ge solute concentration in the liquid Au) at small diameters as the Gibbs-Thomson effect.

3. References

[1] Fröberg, L.E.; Seifert, W.; Johansson J. Diameter Dependent Growth Rate of InAs Nanowires. *Phys. Rev. B* **2007,** *76*, 153401.

[2] Jiang, Q.; Lu, H. M.; Zhao M. Modeling of Surface Energies of Elemental Crystals. *J. Phys.: Condens. Matter.* **2004**, *16*, 521.

[3] Tan, T. Y.; Li, N.; Gosele, U. Is There as Thermodynamic Size Limit of Nanowires Grown by the Vapor-Liquid-Solid Process. *Appl. Phys. Lett.* **2007**, *183*, 1199.

[4] Schmidt, V.; Senz, S.; Gösele, U. *"The shape of Epitaxially grown Si Nanowires and the Influence of the Line Tension",* Appl. Phys. A **2005**, *80*, 445.

[5] Naidich, Y. V.; Perevertailo, V. M.; Obushchak, L. P. Contact Properties of the Phases Participating in the Crystallization of Gold-Silicon and Gold-Germanium Melts. *Poroshkovaya Metallurgia* **1975**, *151*, 63.